KURENAI 紅
Kyoto University Research Information Repository

KYOTO UNIVERSITY

Title	Electronic structures of dynamically stable As2O3, Sb2O3, and Bi2O3 crystal polymorphs
Author(s)	Matsumoto, Akifumi; Koyama, Yukinori; Togo, Atsushi; Choi, Minseok; Tanaka, Isao
Citation	PHYSICAL REVIEW B (2011), 83(21)
Issue Date	2011-06
URL	http://hdl.handle.net/2433/161785
Right	©2011 American Physical Society
Type	Journal Article
Textversion	publisher

Kyoto University

Electronic structures of dynamically stable As$_2$O$_3$, Sb$_2$O$_3$, and Bi$_2$O$_3$ crystal polymorphs

Akifumi Matsumoto,[1] Yukinori Koyama,[1] Atsushi Togo,[1] Minseok Choi,[1] and Isao Tanaka[1,2,3,*]

[1]*Department of Materials Science and Engineering, Kyoto University, Kyoto 606-8501, Japan*
[2]*Nanostructures Research Laboratory, Japan Fine Ceramics Center, Nagoya 456-8587, Japan*
[3]*Fukui Institute for Fundamental Chemistry, Kyoto University, Kyoto 606-8103, Japan*

The relationships between the atomic arrangements, electronic structures, and energetics of three sesquioxides, As$_2$O$_3$, Sb$_2$O$_3$, and Bi$_2$O$_3$, are systematically investigated by first-principles lattice-dynamics calculations. Dynamically stable structures of the defective fluorite family are searched for by including atomic displacements along imaginary modes of lattice vibrations that appear in high-symmetry structures. Experimentally reported crystal structures (arsenolite-As$_2$O$_3$, α-Sb$_2$O$_3$, β-Sb$_2$O$_3$, and β-Bi$_2$O$_3$) are found to be formed by symmetry breaking and local atomic distortion in this way. Moreover, some dynamically stable structures that have not yet been revealed by experiments are discovered. Their electronic structures and the magnitudes of their band gaps are obtained. In the dynamically stable low-symmetry structures, valence electrons localize and form an asymmetric charge distribution along the direction of an empty anion site of the defective fluorite structure. This is a common characteristic of a "lone pair" of cations. The formation of the lone pair is less significant in the order As$_2$O$_3$, Sb$_2$O$_3$, Bi$_2$O$_3$, which is the same trend as the lattice distortion. The formation of the lone pair plays an essential role in determining the structures, stability, and properties of these sesquioxides.

I. INTRODUCTION

Crystal structures of simple metal oxides are often composed of a close-packed oxide-ion sublattice with its tetrahedral or octahedral interstitial sites occupied by cations. Sesquioxides of late group-15 elements in the Periodic Table, i.e., As$_2$O$_3$, Sb$_2$O$_3$, and Bi$_2$O$_3$, form several polymorph structures that are far from such simple metal oxides. They form highly distorted structures with large open spaces (or low atomic density). It is generally accepted that the atomic distortion can be ascribed to the presence of "lone pair" electrons, because two ns ($n = 4$, 5, and 6) electrons remain in As^{3+}, Sb^{3+}, and Bi^{3+} in the formal sense, respectively. However, the relationships between their crystal structures, electronic structures, and energetics have not been quantitatively investigated.

It has been experimentally shown that As$_2$O$_3$ exhibits two polymorphs: cubic arsenolite and monoclinic claudetite.[1–4] Sb$_2$O$_3$ is also known to exhibit two polymorphs: cubic α-phase (senarmontite) and orthorhombic β-phase (valentinite).[5–9] Bi$_2$O$_3$ has been reported to form six polymorphs: monoclinic α-phase, tetragonal β-phase, cubic γ-phase, cubic δ-phase, orthorhombic ε-phase, and triclinic ω-phase.[10–20] The structures of these three sesquioxides are closely related. The structure of arsenolite-As$_2$O$_3$ is the same as that of α-Sb$_2$O$_3$. β-Sb$_2$O$_3$ is isostructural to ε-Bi$_2$O$_3$.

The physical properties of crystals are generally strongly dependent on their structures. For example, Bi$_2$O$_3$ exhibits high oxide ionic conductivity in the δ phase while the other phases show very low ionic conductivity.[21] Understanding the property-structure relationships is therefore essential for the selection of materials. Although these three sesquioxides have similarities in their structures, systematic studies on them have not been reported. In this study, the energetics and crystal and/or electronic structures of M_2O$_3$ ($M =$ As, Sb, Bi) polymorphs are systematically investigated by first-principles calculations.

The structures of these sesquioxides appear to be quite diverse. However, a major part of them can be included in a defective fluorite family, which is based on a fluorite structure in which a quarter of the O sites are vacant. The term "array" will be used hereafter to refer to the atomic arrangement in the O sites of the fluorite structure, while the term "arrangement" will retain its general meaning and refer to a set of specific atomic positions. Arsenolite-As$_2$O$_3$ and α-Sb$_2$O$_3$ are classified into the $\langle 111 \rangle$ array model, in which the vacant sites are aligned in the $\langle 111 \rangle$ direction. β-Bi$_2$O$_3$ is classified into the $\langle 100 \rangle$ array model, in which the vacant sites are aligned in the $\langle 100 \rangle$ direction. β-Sb$_2$O$_3$ and ε-Bi$_2$O$_3$ are classified into the valentinite-type array model, which is made by doubling the defective fluorite unit cell with the [100] array in the [001] direction along with the translation of the vacancy array by half the unit-cell size in the [010] direction. In our previous report,[22] the structures of defective fluorite Bi$_2$O$_3$ family members were investigated in detail. A series of dynamically stable structures was found by lowering the symmetry along imaginary modes of lattice vibrations from the high-symmetry defective fluorite structure. The experimentally reported structure of β-Bi$_2$O$_3$[20] was obtained from the high-symmetry $\langle 100 \rangle$ array model in this way. It was also emphasized that the clear band gap of Bi$_2$O$_3$ can be found only when such symmetry breaking is included for the $\langle 100 \rangle$, $\langle 110 \rangle$, and $\langle 111 \rangle$ array models. In the present study, we search for dynamically stable structures of As$_2$O$_3$ and Sb$_2$O$_3$ in the same manner as we did for those of Bi$_2$O$_3$, as described in our previous report.[22] Then the electronic origin of their structures and energetics is discussed.

II. COMPUTATIONAL PROCEDURES

Five array models based on the defective fluorite structure ($\langle 100 \rangle$, $\langle 110 \rangle$, $\langle 111 \rangle$, bixbyite-type, and valentinite-type array models) were examined for the three sesquioxides. The five
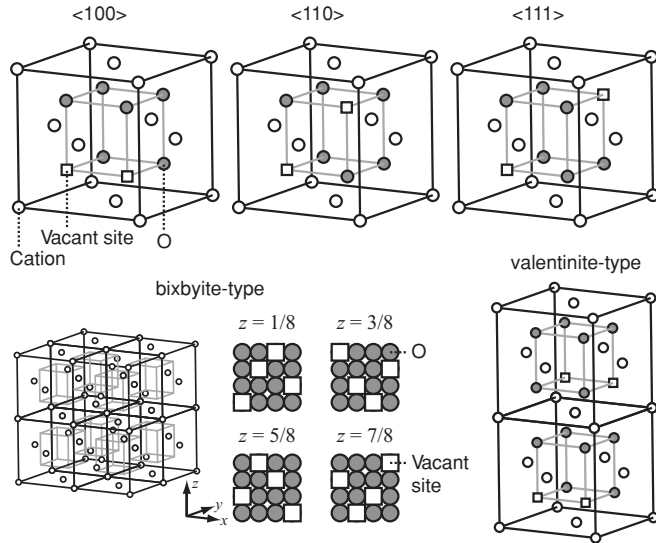
FIG. 1. The five array models of the defective fluorite structure. Since the bixbyite-type array is complicated, the array in each layer is drawn to the right.

array models of the defective fluorite structure are shown in Fig. 1. Bixbyite- and valentinite-type array models can be made in the $2\times2\times2$ and $1\times1\times2$ supercells of the defective fluorite unit cell, respectively. For comparison, two different kinds of atomic arrangements within the monoclinic space group of $P2_1/c$ were examined, which were taken from experimentally reported structures of claudetite-As_2O_3 (Ref. 23) and α-Bi_2O_3.[24]

The first-principles calculations were performed by the projector augmented wave (PAW) method[25] implemented in the VASP code.[26–28] The exchange-correlation term was treated with the Perdew-Burke-Ernzerhof (PBE) functional based on the generalized gradient approximation (GGA).[29] Plane waves were used as the basis functions with a cutoff energy of 360 eV. The convergence of the formation energy with respect to the plane-wave cutoff was found to be better than 0.01 eV/formula unit. The radii of the PAW potentials were 1.11, 1.21, 1.32, and 0.98 Å for As, Sb, Bi, and O, respectively. The $4s$ and $4p$ electrons for As; $5s$ and $5p$ electrons for Sb; $5d$, $6s$, and $6p$ electrons for Bi; and $2s$ and $2p$ electrons for O

were treated as valence and the remaining electrons were kept frozen. In the calculation of the charge density in Sec. III D, the $5d$ electrons of Bi were kept frozen to match the number of valence electrons with that of As and Sb. Integration in the reciprocal space was performed by the Monkhorst-Pack scheme[30] using the $4\times4\times4$ mesh for the $\langle100\rangle$, $\langle110\rangle$, and $\langle111\rangle$ array models, the $4\times4\times2$ mesh for the valentinite-type array model, the $2\times2\times2$ mesh for the bixbyite-type array model, the $3\times6\times2$ mesh for the claudetite-As_2O_3 model, and the $3\times2\times2$ mesh for the α-Bi_2O_3 model. The total energy was minimized until the energy convergence became less than 1×10^{-5} eV.

To examine the stability of the model structures against lattice dynamics, the force-constant approach involving a finite displacement was used employing the FROPHO code.[31–33] The $2\times2\times2$ supercells of the defective fluorite structure were used with a displacement of 0.01 Å along the x, y, and z directions for each atom.

III. RESULTS AND DISCUSSION

A. Symmetry breaking from ideal defective fluorite structures

First a set of defective fluorite structures with the five different array models was optimized by imposing the highest symmetry that can accommodate the array of vacant sites in each defective fluorite structure. Then the $\langle111\rangle$ and bixbyite-type array models formed a cubic lattice, the $\langle100\rangle$ and $\langle110\rangle$ array models formed a tetragonal lattice, and the valentinite-type array model formed an orthorhombic lattice. These will be referred to hereafter as high-symmetry (HS) structures. Lattice-dynamics calculations were performed for these structures. Examples of phonon band structures for the $\langle111\rangle$ array models of the three sesquioxides are shown in Fig. 2. An imaginary value of the frequency illustrated below 0 indicates that the structure is at a local maximum of the potential surface and is unstable against the corresponding lattice vibration. All the HS defective fluorite structures of the three sesquioxides with the five different arrays show such imaginary frequencies and thus are dynamically unstable.

These HS structures were distorted by adding atomic displacements of less than 0.5 Å according to the vibration mode with the largest absolute value of the imaginary frequency. This
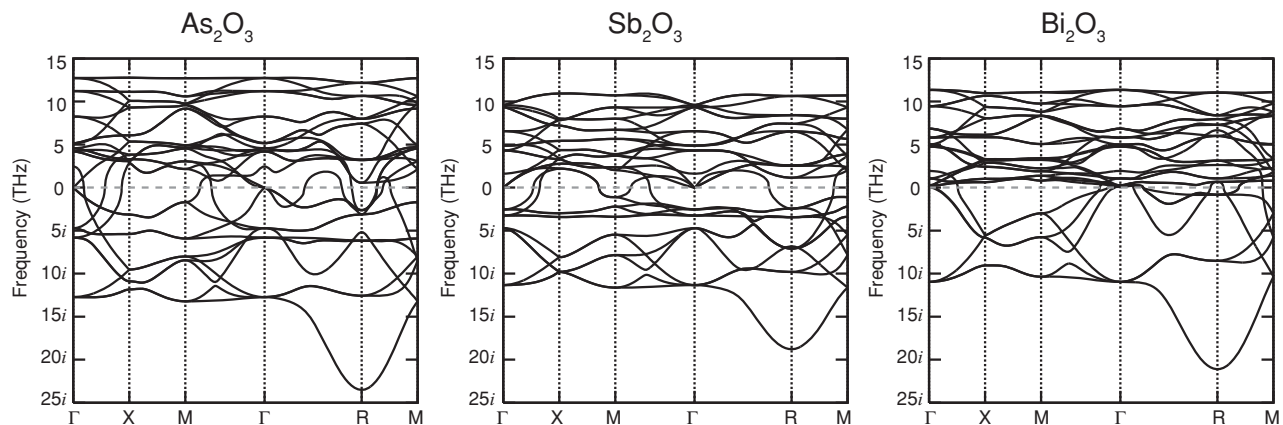

FIG. 2. Phonon band structures of the $\langle111\rangle$-HS arrangements of the three sesquioxides.

TABLE I. Details of calculated LS structures compared with experimentally reported structures of As_2O_3.

<100>-LS-As_2O_3				
Space Group	$P4_2/n$ (No. 86)			
Lattice Parameter	$a = 7.04$Å $c = 8.31$Å			
Atom Coordinate	As (1) 8g	0.047	0.274	0.604
	O (1) 8g	0.158	0.183	0.420
	O (2) 4e	0	0.5	0.002

valentinite-LS-As_2O_3				
Space Group	$Pcc2$ (No. 27)			
Lattice Parameter	$a = 12.57$Å $b = 5.99$Å $c = 5.25$Å			
Atom Coordinate	As (1) 4e	0.120	0.357	0.494
	As (2) 4e	0.380	0.143	0.420
	O (1) 2b	0	0.5	0.115
	O (2) 2c	0.5	0	0.114
	O (3) 4e	0.316	0.081	0.301
	O (4) 4e	0.184	0.581	0.301

<111>-LS-A_2O_3				
Space Group	$Fd\bar{3}m$ (No. 227)			
Lattice Parameter	$a = 11.54$Å			
Atom Coordinate	As (1) 32e	0.899	0.899	0.899
	O (1) 48f	0.172	0	0

arsenolite (experimental data[1])				
Space Group	$Fd\bar{3}m$ (No. 227)			
Lattice Parameter	$a = 11.07$Å			
Atom Coordinate	As (1) 32e	0.897	0.897	0.897
	O (1) 48f	0.173	0	0

claudetite-As_2O_3				
Space Group	$P2_1/c$ (No. 14)			
Lattice Parameter	$a = 9.82$Å $b = 4.69$Å $c = 14.05$Å $\beta = 144.47°$			
Atom Coordinate	As (1) 4e	0.681	0.835	0.382
	As (2) 4e	0.182	0.299	0.818
	O (1) 4e	0.608	0.460	0.322
	O (2) 4e	0.955	0.149	0.769
	O (3) 4e	0.394	0.358	0.033

claudetite (experimental data[23])				
Space Group	$P2_1/c$ (No. 14)			
Lattice Parameter	$a = 9.11$Å $b = 4.64$Å $c = 13.28$Å $\beta = 143.90°$			
Atom Coordinate	As (1) 4e	0.685	0.831	0.383
	As (2) 4e	0.188	0.292	0.816
	O (1) 4e	0.614	0.459	0.333
	O (2) 4e	0.946	0.140	0.762
	O (3) 4e	0.401	0.349	0.034

atomic displacement lowered the symmetry. The structures were then optimized again with the new symmetry.

The lattice-dynamics calculations were performed on the newly obtained structures. If the imaginary mode still remained, the same procedure was repeated until it disappeared at all commensurate points in the reciprocal space of the given cell. Commensurate points correspond to the wave vectors commensurate with the periodicity of the cell under examination. A thus obtained dynamically stable structure showing no imaginary modes at the commensurate points,

is hereafter referred to as a low-symmetry (LS) structure. Note that both the new arrangement and the original arrangement are classified into the same array model. However, the symmetry is lower in the new arrangement. If the atomic displacements during the geometric optimization were too large to be described within the same oxygen atomic array model, the procedure was terminated.

The ⟨111⟩-HS arrangement of As_2O_3, which is obtained by optimizing the ideal defective fluorite structure with its symmetry, exhibits various imaginary modes as shown in

TABLE II. Details of calculated LS structures compared with experimentally reported structures of Sb_2O_3.

		$\langle 111 \rangle$-LS-Sb_2O_3				α-Sb_2O_3 (experimental data[6])		
Space Group		$Fd\bar{3}m$ (No. 227)				$Fd\bar{3}m$ (No. 227)		
Lattice Parameter		$a = 11.42$Å				$a = 11.15$Å		
Atom Coordinate	Sb (1)	32e	0.887	0.887	0.887	Sb (1)	32e	0.885	0.885	0.885
	O (1)	48f	0.186	0	0	O (1)	48f	0.186	0	0

		valentinite-LS-Sb_2O_3				β-Sb_2O_3 (experimental data[6])		
Space Group		$Pccn$ (No. 56)				$Pccn$ (No. 56)		
Lattice Parameter		$a = 5.20$Å $b = 12.56$Å $c = 5.52$Å				$a = 4.91$Å $b = 12.46$Å $c = 5.41$Å		
Atom Coordinate	Sb (1)	8e	0.053	0.127	0.180	Sb (1)	8e	0.041	0.127	0.178
	O (1)	8e	0.25	0.25	0.018	O (1)	8e	0.25	0.25	0.023
	O (2)	4c	0.151	0.057	0.857	O (2)	4c	0.152	0.059	0.855

		claudetite-Sb_2O_3		
Space Group		$P2_1/c$ (No. 14)		
Lattice Parameter		$a = 9.73$Å $b = 4.87$Å $c = 14.51$Å $\beta = 146.56°$		
Atom Coordinate	Sb (1)	4e	0.710	0.855	0.408
	Sb (2)	4e	0.207	0.330	0.809
	O (1)	4e	0.621	0.462	0.336
	O (2)	4e	0.988	0.176	0.795
	O (3)	4e	0.443	0.400	0.049

Fig. 2. The displacement along the strongest imaginary mode leads to the $\langle 111 \rangle$-LS arrangement. The symmetry and atomic coordinates of the $\langle 111 \rangle$-LS arrangement of As_2O_3 were found to be in good agreement with the experimentally reported structure of arsenolite-As_2O_3.[1] In the other array models, dynamically stable $\langle 100 \rangle$-LS and valentinite-LS arrangements were found. Table I shows the details of the calculated LS structures and experimentally reported structures of As_2O_3.

For Sb_2O_3, the $\langle 111 \rangle$-HS and valentinite-HS arrangements change to dynamically stable $\langle 111 \rangle$-LS and valentinite-LS arrangements, respectively. They are isostructural to the experimentally reported structures of α-Sb_2O_3 and β-Sb_2O_3.[5]

The structural data of the dynamically stable arrangements and experimentally reported structures are shown in Table II.

In addition to the sets of defective fluorite structures, two different kinds of monoclinic structures with the space group of $P2_1/c$ were examined. The energy of the claudetite-As_2O_3-type arrangement is lower than that of the α-Bi_2O_3-type arrangement by 0.23 eV/f.u. in As_2O_3 and by 0.12 eV/f.u. in Sb_2O_3. On the other hand, the α-Bi_2O_3-type arrangement is more stable than the claudetite-As_2O_3-type arrangement by 0.13 eV/f.u. in Bi_2O_3. The energetically lower structure is hereafter referred to as the $P2_1/c$ model of each sesquioxide. These $P2_1/c$ models were found to be dynamically stable. The
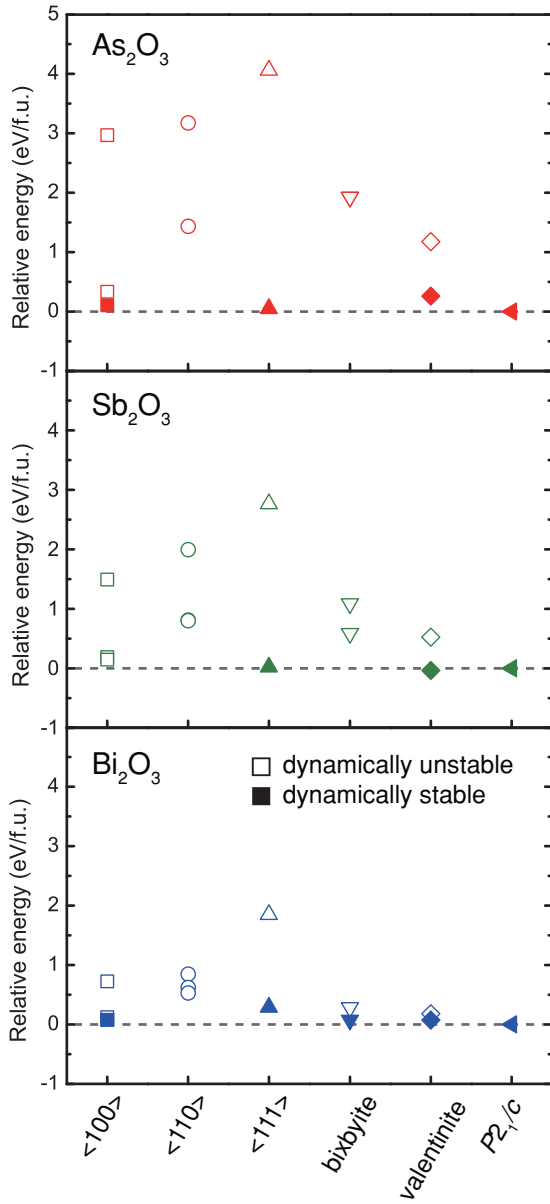
FIG. 3. (Color online) Energies of each arrangement relative to the monoclinic $P2_1/c$ structure.

energies of each arrangement relative to the $P2_1/c$ models are summarized in Fig. 3. The open marks correspond to the dynamically unstable arrangements, and the solid marks correspond to the dynamically stable LS arrangements.

In As_2O_3, three of the dynamically stable defective fluorite structures ($\langle 100 \rangle$-LS, $\langle 111 \rangle$-LS, and valentinite-LS arrangements) exhibit relative energies of less than 0.1 eV/f.u. Although arsenolite-As_2O_3 is the low-temperature phase according to an experimental report,[34] the corresponding arrangement, $\langle 111 \rangle$-LS, has 0.05 eV/f.u. higher energy than the claudetite-As_2O_3-type arrangement. Similarly to As_2O_3, the energetic hierarchy between α-Sb_2O_3 and β-Sb_2O_3 according to the present calculations does not agree with experimental one. The relative energy of the low-temperature phase (α-Sb_2O_3), which corresponds to the $\langle 111 \rangle$-LS arrangement, is 0.06 eV/f.u. higher than that of the high-temperature phase
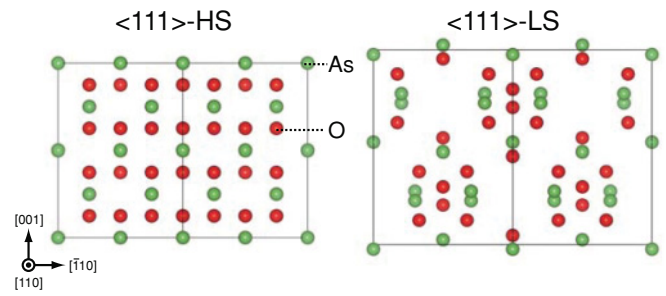
(β-Sb_2O_3), which corresponds to the valentinite-LS arrangement. The origin of this inconsistency in the energetic hierarchy is not yet clear. It may be related either to the presence of some defects or disordering in the phases of interest, or the choice of exchange-correlation functional in the DFT calculations. In fact, the relative energy of α-Sb_2O_3 became 0.004 eV/f.u. lower than that of β-Sb_2O_3 when we used the Heyd-Scuseria-Ernzerhof (HSE06)[35–37] hybrid functional for the same calculation. More detailed study is required in the future to discuss the detailed energetic hierarchy among polymorphs, which is beyond the scope of the present study.

Some of the dynamically stable structures found in the present study have not yet been revealed by experiments. They are $\langle 100 \rangle$-LS and valentinite-LS for As_2O_3, claudetite-type for Sb_2O_3, and $\langle 111 \rangle$-LS, bixbyite-LS, and valentinite-LS

FIG. 4. (Color online) Projection of the $\langle 111 \rangle$-HS and -LS arrangements of As_2O_3 from the [110] direction.
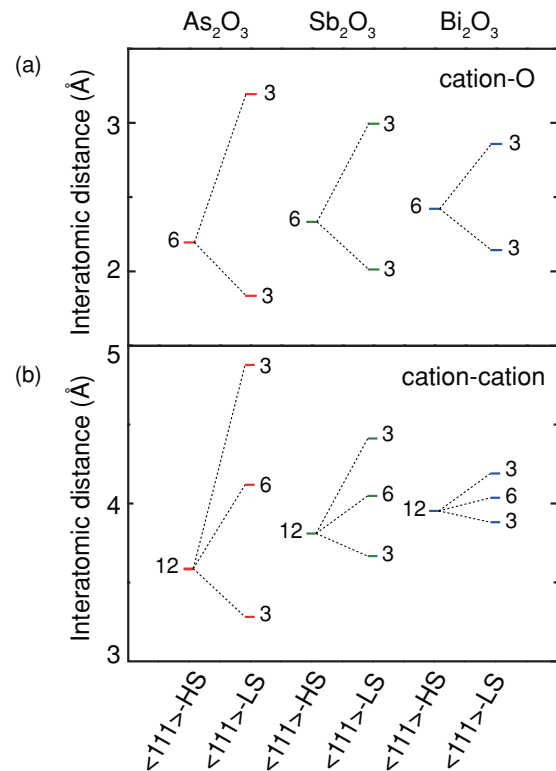

FIG. 5. (Color online) (a) Cation-O and (b) cation-cation interatomic distances in the $\langle 111 \rangle$-HS and -LS arrangements of the three sesquioxides. The numbers beside the bars show the degeneracy.
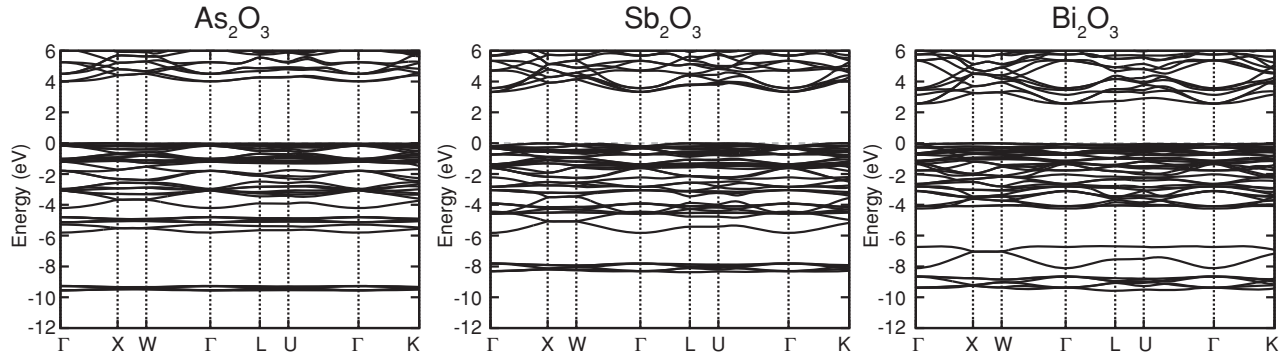
FIG. 6. Electronic band structures of the ⟨111⟩-LS arrangements for the three sesquioxides. The top of the valence band is set to 0 on the vertical axis.

for Bi_2O_3. With the exception of ⟨111⟩-LS for Bi_2O_3, their formation energies are within 0.1 eV/f.u. of that for the structure with the lowest energy, implying the high probability of formation under controlled experimental conditions.

B. Local atomic arrangements of dynamically stable structures

As described in the previous section, the energy of each array model is lowered considerably upon symmetry breaking and local atomic distortion. In this section, the local atomic arrangements of the stable structures are investigated.

Among the five array models based on the defective fluorite structure, the ⟨111⟩-LS arrangements of the three sesquioxides have the same space group. The ⟨111⟩-HS arrangement has the $Pn\bar{3}m$ space group with a 10-atom unit cell. It transforms to the ⟨111⟩-LS arrangement, which has the $Fd\bar{3}m$ space group with an 80-atom unit cell, in the three sesquioxides. We therefore compare the HS and LS arrangements of the three sesquioxides with the ⟨111⟩ array model in detail. Both HS and LS arrangements have one cation site and one O site. The cation is coordinated by six O ions and twelve cations. Figure 4 shows the ⟨111⟩-HS and -LS arrangements of As_2O_3

from the [110] direction. As can be clearly seen in Fig. 4, ions tend to aggregate in the LS arrangement, while they are evenly distributed in the HS arrangement. Similar trends can be observed in Sb_2O_3 and Bi_2O_3. Figure 5 shows (a) cation-O and (b) cation-cation interatomic distances in the ⟨111⟩-HS and -LS arrangements of the three sesquioxides. The numbers beside the bars show the degeneracy. All cation-O and cation-cation interatomic distances are the same in the HS arrangement. However, in the LS arrangement some of them are shortened and others are elongated by the local distortion. The volume also changes with the structural change. Table III shows the lattice constant and the volume expansion of the 80-atom cubic-cell in the ⟨111⟩-HS and -LS arrangements for the three sesquioxides. The volume increases by 47% in As_2O_3, but only by 6% in Bi_2O_3. With increasing atomic aggregation and volume, the atomic density locally decreases in the ⟨111⟩-LS arrangement.
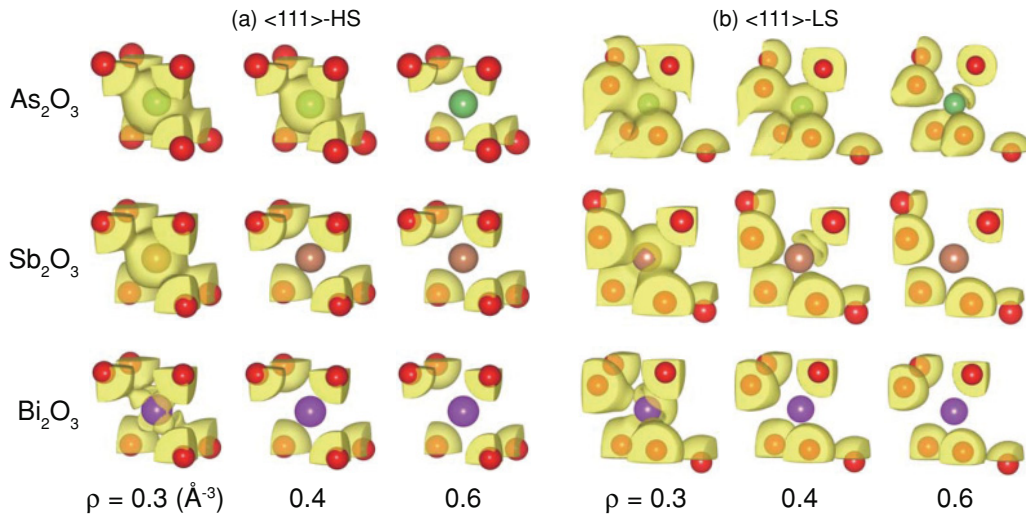

FIG. 7. (Color online) Isosurfaces of the valence electron density distribution around the cation in the (a) ⟨111⟩-HS and (b) ⟨111⟩-LS arrangements of the three sesquioxides. Part of the unit cell is extracted. Red spheres are oxygen ions. Green, brown, and violet spheres are cations.

TABLE III. Lattice constant and volume expansion of 80-atom cubic-cell in the ⟨111⟩-HS and -LS arrangements of the three sesquioxides.

	⟨111⟩-HS	⟨111⟩-LS	Volume expansion
As_2O_3	10.13 Å	11.54 Å	47%
Sb_2O_3	10.77 Å	11.42 Å	19%
Bi_2O_3	11.18 Å	11.41 Å	6%

C. Electronic structures of dynamically stable structures

Sb_2O_3 and Bi_2O_3 have been experimentally found to have clear band gaps.[38–41] Although details of the measurement were not given, As_2O_3 has also been reported to have a band gap.[42] In spite of these reports, the HS structures with a 10-atom unit cell, i.e., the ⟨100⟩-HS, ⟨110⟩-HS, and ⟨111⟩-HS arrangements, for the three sesquioxides have either a metallic or semimetallic electronic structure in which an energy band crosses the Fermi level or the top of the valence band is higher than the bottom of the conduction band. When symmetry breaking and local distortion are introduced into these structures, band gaps appear. The electronic band structures of the ⟨111⟩-LS arrangements for the three sesquioxides are shown in Fig. 6. All LS arrangements for the three sesquioxides have clear band gaps, which are summarized in Table IV. Since the LS arrangement could not be obtained in some of the array models, some values are missing. α-Sb_2O_3 and β-Sb_2O_3 have been reported to have band gaps of 4 eV (Refs. [38–40]) and 3.3 eV,[38] respectively. The corresponding theoretical values in this work are 3.33 eV (⟨111⟩-LS) and 2.20 eV (valentinite-LS), respectively. The underestimation may be ascribed to the use of the GGA for the exchange-correlation functional. As a matter of fact, the band gaps similarly calculated with the HSE06 hybrid functional are 4.28 eV (⟨111⟩-LS) and 3.60 eV (valentinite-LS), respectively, which are much closer to the experimental results. The band structures by the HSE06 calculations are seemingly the same as those by the GGA except for the improved band gap.

We found a trend that the band gap decreases with the increase of the relative energy among the different arrangements. The local distortion affects the electronic structure significantly. The inclusion of symmetry breaking and local distortion is therefore essential for accurately describing the energetics and electronic structures of the three sesquioxides.

D. Formation of a "lone pair"

In the sesquioxides of late group-15 elements, two ns electrons remain in the valence band in the formal sense. When they are localized to the cations and form an asymmetric charge distribution, they are referred to 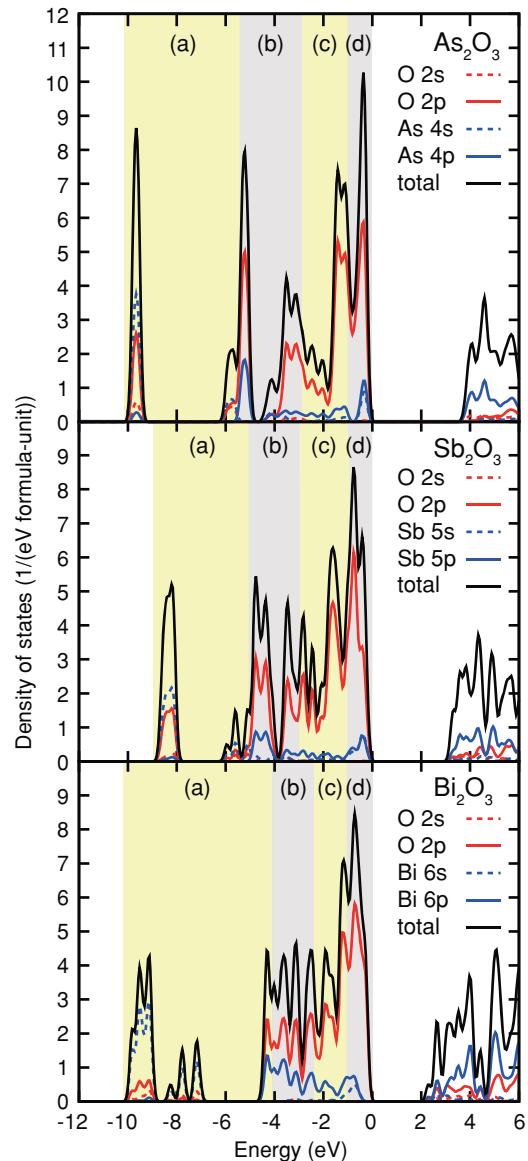as a "lone pair". The formation of a lone pair often plays a central role in determining the local atomic arrangement. To examine the origin of the local atomic distortion and symmetry breaking, we examine the charge distribution of the sesquioxides in detail.

FIG. 8. (Color online) Partial electron density of states of the ⟨111⟩-LS arrangement for the three sesquioxides. The top of the valence band is set to 0. The black line represents the total density of states. Broken and solid red lines show the O 2s and O 2p states, respectively. Broken and solid blue lines represent the cation ns and np states, respectively. Four regions, (a)–(d), include the same number of valence electrons.

TABLE IV. Calculated GGA band gaps of LS structures. Values in square brackets are HSE06 band gaps. The unit is an electronvolt.

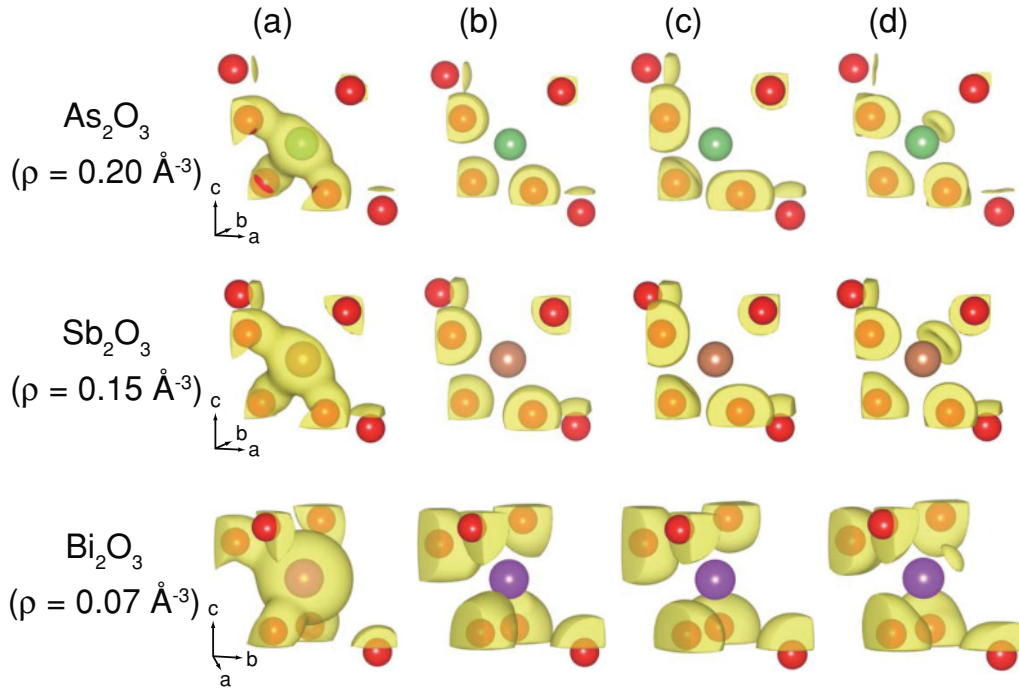|	⟨100⟩-LS	⟨111⟩-LS	bixbyite-LS	valentinite-LS	$P2_1/c$
As_2O_3		4.01 [5.34]		3.23 [3.92]	3.58
Sb_2O_3		3.33 [4.28]		2.20 [3.60]	2.51
Bi_2O_3	1.61 [2.73]	2.57 [3.93]	2.58	1.74 [2.89]	2.29

FIG. 9. (Color online) Isosurface of the valence electron density distribution in each region (see Fig. 8) around the cation in the $\langle 111 \rangle$-LS arrangement of the three sesquioxides. The isosurfaces of 0.20, 0.15, and 0.07 Å^{-3} are shown for As_2O_3, Sb_2O_3, and Bi_2O_3, respectively. Red spheres are oxygen ions. Green, brown, and violet spheres are cations.

Figure 7 shows the isosurfaces of the valence electron density distribution around the cation in the $\langle 111 \rangle$-HS and -LS arrangements of the three sesquioxides. The atomic arrangements can be better visualized in the HS arrangement. The cation is coordinated by six O ions and two empty sites. The empty sites are located at the front-bottom-left and top-right-back in the cubic structure shown in Fig. 7(a). In the transformation from HS to LS, O ions move toward the empty site at the front-bottom-left as can be seen in Fig. 7(b). Then the other empty site at the top-right-back has a larger open space than the corresponding space in the HS arrangement. In the HS arrangement, electrons are spherically distributed around the cation, as shown in Fig. 7(a). The isosurfaces of $\geqslant 0.6$ Å^{-3} for As_2O_3, $\geqslant 0.4$ Å^{-3} for Sb_2O_3, and $\geqslant 0.3$ Å^{-3} for Bi_2O_3 cannot be seen around the cation. On the other hand, as shown in Fig. 7(b), the charge density around the cation became asymmetric and more localized in the LS arrangements. The charge distribution along the direction of the empty site at the top-back-right can be clearly seen in the isosurfaces of 0.6 Å^{-3} for As_2O_3, 0.4 Å^{-3} for Sb_2O_3, and 0.3 Å^{-3} for Bi_2O_3.

To inspect the formation of the lone pair in more detail, the partial charge-density distribution is investigated. Figure 8 shows the electron density of states in the $\langle 111 \rangle$-LS arrangement for the three sesquioxides. The top of the valence band is set to zero. The valence band is mainly composed of the O $2p$ state with minor contributions of the cation ns and np states ($n = 4$, 5, and 6 for As, Sb, and Bi, respectively). When the fully filled $(n-1)d$ electrons of the cations are excluded, the three sesquioxides have $2 \times 2 + 3 \times 6 = 22$ valence electrons in the O $2p$ band per formula unit of M_2O_3. The O $2p$ band is divided into four regions, (a)–(d), to include the same number of electrons, $22/4$, in each region as shown in Fig. 8.

The highest-energy region, (d), is mainly composed of O $2p$ states forming an antibonding interaction with the cation nsp state. The isosurface of the partial valence electron density distribution in each region is shown in Fig. 9. The isosurfaces of 0.20, 0.15, and 0.07 Å^{-3} are shown for As_2O_3, Sb_2O_3, and Bi_2O_3, respectively. The model of Bi_2O_3 in Fig. 9 is slightly tilted from the other two models for easy visualization of the electron localization. As shown in Fig. 9, only the isosurface of region (d) is elongated toward the direction of the empty site in all three sesquioxides. This indicates that the cation ns and np electrons in region (d) contribute significantly to the anisotropic and localized charge distribution, which is consistent with the idea of a lone pair on the cation. The magnitudes of the anisotropy and localization become less significant in the order As_2O_3, Sb_2O_3, and Bi_2O_3. This is the same trend as the lattice distortion associated with the $\langle 111 \rangle$-HS to -LS transformation. This means that the formation of the lone pair is most significant in As_2O_3. The formation of the lone pair is thus confirmed to play a central role in the local atomic distortion and symmetry breaking.

IV. SUMMARY

First-principles lattice-dynamics calculations were systematically performed for M_2O_3 ($M =$ As, Sb, Bi). Dynamically stable LS structures were searched for, including atomic displacements along imaginary modes of lattice vibrations that appear in HS defective fluorite structures. The atomic arrangements, electronic structures, and energetics of the LS structures were then examined in detail. The major results in this study can be summarized as follows:

(i) All five array models with the HS defective fluorite arrangements were dynamically unstable against various vibration modes. When symmetry breaking and local distortion were included, some structures became dynamically stable. The majority of the experimentally reported structures (arsenolite-As_2O_3, α-Sb_2O_3, β-Sb_2O_3, and β-Bi_2O_3) were obtained by this procedure. At the same time, some dynamically stable structures not yet revealed by experiments were discovered. They are $\langle 100 \rangle$-LS and valentinite-LS for As_2O_3, claudetite-type for Sb_2O_3, and $\langle 111 \rangle$-LS, bixbyite-LS, and valentinite-LS for Bi_2O_3. With the exception of $\langle 111 \rangle$-LS for Bi_2O_3, their formation energies were within 0.1 eV/f.u. of that for the structure with the lowest energy, implying a high probability of formation under controlled process conditions (Fig. 3).

(ii) Ions tend to aggregate in the LS arrangement, whereas they are evenly distributed in the HS arrangement (Fig. 4). All cation-anion and cation-cation interatomic distances were the same in the HS arrangement. However, in the LS arrangement some of them were shortened and others were elongated by the local distortion (Fig. 5). With increasing atomic aggregation and volume, the atomic density locally decreases in the LS arrangement.

(iii) Although the HS arrangements for the three sesquioxides exhibited either a metallic or semimetallic electronic structure, all LS arrangements exhibited clear band gaps

(Table IV), in good agreement with experimental reports. The inclusion of symmetry breaking and local distortion is therefore essential for accurately describing the energetics and electronic structures of the three sesquioxides.

(iv) In the HS arrangements, electrons are spherically distributed around the cation. On the other hand, in the LS arrangements, the charge density around the cation became asymmetric and elongated along the direction of the empty site (Fig. 7). The cation ns and np ($n = 4$, 5, and 6 for As, Sb, and Bi, respectively) electrons near the top of the valence band contribute significantly to the anisotropic and localized charge distribution (Fig. 9), i.e., the formation of the lone pair. This became less significant in the order As_2O_3, Sb_2O_3, and Bi_2O_3, which was the same trend as the lattice distortion. The formation of the lone pair was thus confirmed to play a central role in the local atomic distortion and symmetry breaking.

*tanaka@cms.mtl.kyoto-u.ac.jp

[1] F. Pertlik, Czech. J. Phys. B **28**, 170 (1978).

[2] A. J. Frueh, Am. Mineral. **36**, 833 (1951).

[3] F. Pertlik, Monatsh. Chem. **109**, 277 (1978).

[4] D. Ležal and K. Koňak, J. Non-Cryst. Solids **192&193**, 187 (1995).

[5] C. Svensson, Acta. Crystallogr., Sect. B **30**, 458 (1974).

[6] C. Svensson, Acta. Crystallogr., Sect. B **31**, 2016 (1975).

[7] S. J. Gilliam, J. O. Jensen, A. Banerjee, D. Zeroka, S. J. Kirkby, and C. N. Merrowa, Spectrochim. Acta Part A **60**, 425 (2004).

[8] R. G. Orman and D. Holland, J. Solid State Chem. **180**, 2587 (2007).

[9] E. I. Voit, A. E. Panasenko, and L. A. Zemnukhova, J. Struct. Chem. **50**, 60 (2009).

[10] M. Drache, P. Roussel, and J. Wignacourt, Chem. Rev. **107**, 80 (2007).

[11] N. M. Sammes, G. A. Tompsett, H. Näfe, and F. Aldinger, J. Eur. Ceram. Soc. **19**, 1801 (1999).

[12] L. G. Sillen, Ark. Kemi **12A**, 1 (1937).

[13] V. G. Gattow and H. Schröder, Z. Anorg. Allg. Chem. **318**, 176 (1962).

[14] V. G. Gattow and D. Schutze, Z. Anorg. Allg. Chem. **328**, 44 (1964).

[15] E. M. Levin and R. S. Roth, J. Res. Natl. Bur. Stand. **68A**, 197 (1964).

[16] H. A. Harwig and A. G. Gerards, Thermochim. Acta **28**, 121 (1979).

[17] C. N. R. Rao, G. V. S. Rao, and S. Ramdas, J. Phys. Chem. **73**, 672 (1969).

[18] N. Cornei, N. Tancret, F. Abraham, and O. Mentré, Inorg. Chem. Commun. **45**, 4886 (2006).

[19] A. F. Gualtieri, S. Imovilli, and M. Prudenziati, Powder Diff. **12**, 90 (1997).

[20] S. K. Blower and C. Greaves, Acta Crystallogr. C **44**, 587 (1988).

[21] T. Takahashi, H. Iwahara, and Y. Nagai, J. Appl. Electrochem. **2**, 97 (1972).

[22] A. Matsumoto, Y. Koyama, and I. Tanaka, Phys. Rev. B **81**, 094117 (2010).

[23] F. Pertlik, Monatsh. Chem. **106**, 755 (1975).

[24] H. A. Harwig, Z. Anorg. Allg. Chem. **444**, 151 (1978).

[25] P. E. Blöchl, Phys. Rev. B **50**, 17953 (1994).

[26] G. Kresse and J. Hafner, Phys. Rev. B **47**, R558 (1993).

[27] G. Kresse and J. Furthmüller, Phys. Rev. B **54**, 11169 (1996).

[28] G. Kresse and J. Furthmüller, Comput. Mater. Sci. **6**, 15 (1996).

[29] J. P. Perdew, K. Burke, and M. Ernzerhof, Phys. Rev. Lett. **77**, 3865 (1996).

[30] H. J. Monkhorst and J. D. Pack, Phys. Rev. B **13**, 5188 (1976).

[31] A. Togo, [http://fropho.sourceforge.net/].

[32] A. Togo, F. Oba, and I. Tanaka, Phys. Rev. B **77**, 184101 (2008).

[33] A. Togo, F. Oba, and I. Tanaka, Phys. Rev. B **78**, 134106 (2008).

[34] K. A. Becker, K. Plieth, and I. N. Stranski, Z. Anorg. Allg. Chem. **266**, 293 (1951).

[35] J. Heyd, G. E. Scuseria, and M. Ernzerhof, J. Chem. Phys. **118**, 8207 (2003).

[36] A. V. Krukau, O. A. Vydrov, A. F. Izmaylov, and G. E. Scuseria, J. Chem. Phys. **125**, 224106 (2006).

[37]J. Heyd, G. E. Scuseria, and M. Ernzerhof, J. Chem. Phys. **124**, 219906 (2006).

[38]C. Wood, B. V. Pelt, and A. Dwight, Phys. Status Solidi B **54**, 701 (1972).

[39]N. Tigau, V. Ciupina, and G. Prodan, J. Cryst. Growth **277**, 529 (2005).

[40]N. Tigau, V. Ciupina, and G. Prodan, J. Optoelectron. Adv. Mater. **8**, 37 (2006).

[41]H. T. Fan, S. S. Pan, X. M. Teng, C. Ye, and G. H. Li, J. Phys. D **39**, 1939 (2006).

[42]J. Portier, G. Campet, C. W. Kwon, J. Etourneau, and M. A. Subramanian, J. Int. J. Inorg. Mater. **3**, 1091 (2001).